Simulation of point defects and threshold displacements in pure Cu and a dilute Cu-Au alloy

Hui-fang Deng and David J. Bacon

Department of Materials Science and Engineering, The University of Liverpool, P.O. Box 147, Liverpool, L69 3BX, United Kingdom

The influence of solute atoms on point-defect properties and defect generation by radiation damage in alloys is known to be important, and hence it is desirable to understand their effect on the basic mechanisms involved. Most computer modeling of these phenomena has only considered pure metals, but as part of a project to investigate displacement cascades in alloys, we have simulated dilute solutions of gold (Au) in copper (Cu), treating this as a "model" for a heavy, oversized solute alloy system. In the present paper, modified many-body interatomic potentials for the Cu-Au system are described that are suitable for modeling high-energy atomic collisions. The properties of point defects in pure copper and the dilute alloy, including solute-defect binding energies, are presented. The oversized solute has a *larger* binding energy with an interstitial atom than with a vacancy. The displacement threshold energy, E_d, of a Cu atom and a Au atom in the copper matrix has been investigated as a function of primary recoil direction, and the difference between the two species is found to be substantial. Furthermore, the presence of a Au solute has a significant effect on the formation of Frenkel pairs by the replacement-collision-sequence mechanism. These results are discussed in terms of the mass and size difference of Cu and Au atoms.

I. INTRODUCTION

The production and properties of point defects are important for the changes in material properties that accompany radiation damage, and a full understanding of the mechanisms involved has long been the goal of those who wish to model and predict material behavior. Atomic-scale computer simulation is a powerful technique to assist in achieving these ends, but so far nearly all research in this area has concentrated on the pure metals, as indicated in the recent review by Diaz de la Rubia and Phythian.[1] With the exception of some recent modeling of defect production in ordered intermetallics, e.g., Refs. 2–5, little has been done on alloys, yet for obvious technological reasons these are materials of great importance, and the defect mechanisms in them are more complex than in pure metals. The present work represents part of a wider attempt to address this issue as regards the role of solute atoms in defect production in displacement cascades in solid solutions. In this paper, we present basic results for the properties of point defects in a dilute binary alloy and the effects of the solute on the displacement threshold event in such a system. Cascade processes will be dealt with in a later publication.

We consider a solid solution of gold in a copper matrix, with the intention of studying the influence of large, oversized solutes on defect mechanisms. We have chosen this as a "model" binary-alloy system for several reasons. First, there is now a good deal of data on cascades in pure copper from molecular dynamics (MD) simulations.[1,6–8] Second, there is a large mass and size difference between the two elemental species. (The mass numbers are 63.5 and 197 and the lattice parameters are 0.3615 and 0.4078 nm for Cu and Au, respectively.) Third, good interatomic potentials are available for this alloy system. However, we have had to modify these potentials so that they are suitable for high-energy atomic

collisions, as described in the next section. In this paper, we shall consider the limiting case of *one* single Au solute in an otherwise pure Cu lattice. We have computed the formation energy, formation volume, and binding energy for vacancies and interstitial atoms in pure copper and copper with a dilute solution of gold. We have also simulated effects at the threshold for atomic displacements, i.e., at the energy where a recoiling atom has just sufficient energy to leave its site (or to force a neighbor to leave its site) and create a stable Frenkel pair, in pure copper and the alloy. This is an important energy regime because the displacement threshold energy E_d, is a parameter in many theories of defect production. The methods and interatomic potentials used are described in Sec. II. The properties of point defects and threshold displacement energy are presented and discussed in Secs. III and IV, respectively.

II. METHOD AND POTENTIALS

A. Computational method

The MD program used here was a modification of the MOLDY code version 6, initially designed for pure metals.[9] We have extended it to treat alloy systems of up to three atomic species in solution and to run on an Amdahl VP1200 processor. It employs a link-cell method for efficient accounting of neighbor interactions, and uses periodic boundary conditions with flexible, constant-pressure boundaries and a variable time-step algorithm. In order to calculate the static properties of the point defects, the block size was $10\times10\times10$ unit cells (=4000 atoms), and after placing the point defect on a suitable site, the system was relaxed for 250 or 500 time steps, i.e., about 2.5 or 5 ps, under zero temperature and pressure to minimize the potential energy and, hence, determine the stable defect configuration. The way in which the forma-

tion energy and volume was defined is dealt with further in Sec. III A.

In simulations of the displacement threshold, the lattice temperature was 0 K and the computational block was usually cubic and consisted of up to $12 \times 12 \times 12$ unit cells, i.e., 6912 atoms. However, for recoils along the $\langle 100 \rangle$ and $\langle 110 \rangle$ directions, where focused collisions can occur, the block was extended along those directions only and considerable CPU time was saved. A size was chosen to contain all the replacements of the replacement collision sequences (RCS) generated, and consisted of up to $20 \times 4 \times 4$ unit cells ($=1280$ atoms) and $28 \times 28 \times 6$ unit cells ($=18\,816$ atoms) for the $\langle 100 \rangle$ and $\langle 110 \rangle$ events, respectively. The initial MD time step was 10 fs. The atoms were allowed to evolve for 600 time steps (equal to approximately 6 ps) from the start of the recoil event; longer times were usually not necessary since we were concerned with the creation of Frenkel pairs which did not recombine "spontaneously," but for directions where RCS occurred, up to 800 time steps were allowed. If no stable Frenkel defects remained at the end of that time, the simulation was restarted with a higher recoil energy. This process continued until the energy threshold, E_d, for stable Frenkel pair production was established. The increment of energy applied in this procedure was between 0.4 and 9 eV and so E_d quoted here is subject to uncertainties of ± 0.2 to ± 4.5 eV.

B. Interatomic potentials

In the framework of the many-body approach currently used in studies of defects in metals (e.g., Refs. 10 and 11), the energy of an assembly of N atoms is given by

$$E = \frac{1}{2} \sum_{i \neq j = 1}^{N} V_{ij}(x_{ij}) - \sum_{i=1}^{N} F_i(\rho_i) \, , \qquad (1)$$

where V_{ij} is the pairwise interaction potential, usually repulsive, between atoms i and j at separation x_{ij}, and F_i is the embedding part of the energy and leads to cohesion. It is a function of the electron density ρ_i associated with atom i and, therefore, depends in alloys on the species of the atom. In the Finnis-Sinclair formalism used here, $F_i(\rho_i)$ equals $\sqrt{\rho_i}$, which is not only computationally convenient but also justified theoretically within the second-moment approximation of the tight-binding theory (Ackland, Finnis, and Vitek[12]). Thus, F_i has the form

$$F_i = \left[\sum_{j=1}^{N} \Phi_{ij}(x_{ij}) \right]^{1/2} \, , \qquad (2)$$

where $\Phi(x_{ij})$ is a pairwise function.

We have based the interatomic potentials required for this work on those derived by Ackland and Vitek[13] for the Cu-Au system. These are of the Finnis-Sinclair-type and were fitted in their derivation to pure metal, alloy, and some defect properties. However, to provide a better treatment of atomic interactions inside the normal nearest-neighbor distance of $a_0/\sqrt{2}$, where a_0 is the lattice parameter, and to model elastic collisions at recoil energies $\geq E_d$, we have modified the repulsive pair part of

these many-body potentials to fit the pressure-volume relation for the pure metals and alloys, and to smoothly join it to the "universal" screened Coulomb potential of Biersack and Ziegler[14] at small interatomic separation. Since we are only dealing here with the influence of a single Au solute on defect properties and production, we do not need to consider Au-Au interactions in the simulations, but we shall describe the potentials for completeness.

To be specific, if x is the separation of two atoms, then when $x < x_1$ ($x_1 = 1.0$ Å for Cu-Cu or Au-Au homoatoms and $x_1 = 1.2$ Å for Cu-Au heteroatoms), we adopted the pair part,

$$V(x) = [(Z_A Z_B e^2)/(4\pi\varepsilon_0 x)]U(x/a_u) \, , \qquad (3a)$$

with

$$U(y) = 0.1818 \exp(-3.2y) + 0.5099 \exp(-0.9423y)$$
$$+ 0.2802 \exp(-0.4029y)$$
$$+ 0.02817 \exp(-0.2016y) \, , \qquad (3b)$$

and

$$a_u = 0.88534 a_b/(Z_A^{0.23} + Z_B^{0.23}) \, , \qquad (3c)$$

where U is the universal screening function, a_u is the characteristic screening length, a_b is the Bohr radius, $y = x/a_u$, Z_A and Z_B are the atomic numbers of the interacting atoms, and e and ε_0 have their usual meaning. It should be pointed out that the determination of the knot point $x_1 = 1$ or 1.2 Å is based on the fact that the universal potential is more accurate than other forms with a distance of 1 Å (Ref. 15) when compared with the experimental data[16] but it becomes too strong for a distance of $x > 1.5$ Å (Ref. 17). Furthermore, this choice is also consistent with that of others,[18,19] and, therefore, any attempt to modify it in this range of interaction is unwise and also unnecessary.

When $x \geq x_2$ ($x_2 = 2.0$ Å for Cu-Cu and Au-Au, and $x_2 = 2.2$ Å for Cu-Au), the modified versions of Ackland and Vitek's[13] Cu-Cu, Au-Au, and Cu-Au cross potentials were used, which are in the form of cubic splines:

$$V^{AA}(x) = \sum_{k=1}^{6} a_k^{AA} H(r_k^{AA} - x)(r_k^{AA} - x)^3 \, , \qquad (4)$$

$$V^{AB}(x) = \sum_{k=1}^{4} a_k^{AB} H(r_k^{AB} - x)(r_k^{AB} - x)^3 \, , \qquad (5)$$

where A and B stand for, respectively, Cu and Au, and $H(x)$ is the Heaviside unit step function which gives the cutoff distance of each spline segment. V^{BB} has the same cubic spline form as V^{AA}, with a_k^{AA} and r_k^{AA} replaced by a_k^{BB} and r_k^{BB}, respectively. In the original Ackland and Vitek pure Cu potential,[13] the coefficient $a_6^{AA} = 0$. This gives a volume-pressure relation for a single crystal that deviates from experiment at high pressure. In order to improve this, the volume-pressure curve was fitted to experimental data[20] by adjusting the coefficient a_6^{AA} to be 135.0 with $r_6 = 0.707 a_0$ and leaving all other parameters unchanged. The parameters in the original three-point

TABLE I. Potential parameters in Eq. (6) for pure Cu and Au and the Cu-Au alloy, and their valid ranges. These produce $V(x)$ in units of J.

	C_0	$C_1(10^{10}/m)$	$C_2(10^{20}/m^2)$	$C_3(10^{30}/m^3)$	$x_1(\text{Å})$	$x_2(\text{Å})$
Cu-Cu	5.837 638 0	3.544 945 8	−5.848 147 2	1.370 097 4	1.0	2.0
Cu-Au	6.641 387 9	1.722 509 8	−3.668 636 3	0.740 855 02	1.2	2.2
Au-Au	7.355 008 5	3.848 610 0	−6.790 966 1	1.741 673 3	1.0	2.0

cubic spline V^{AB} with $a_4^{AB}=0$ were determined by fitting to the data Cu-Au alloys, and the extra term with $k=4$ was added here within the range less than the nearest-neighbor distance in order to give a better fit to the volume-pressure relationship for the ordered alloy Cu₃Au. It was $a_4=7.5$ eV/a_0^3 with $r_4=2.556\ 191\ 01$ Å.

To link the universal potentials to the modified Ackland-Vitek functions, an exponential form for the pair part of the potential was constructed over the range $x_1 \le x \le x_2$ having the form

$$V(x)=\exp(C_0+C_1x+C_2x^2+C_3x^3)\ ,\qquad (6)$$

where coefficients C_0, C_1, C_2, and C_3 were determined by equating the values of this potential and its first derivative to those of Eqs. (3a) and (4) or (5) at points x_1 and x_2, respectively, and are given in Table I. The choice of $x_2=2$ Å is the same as that chosen in Ref. 19. The resulting pair functions for Cu-Cu, Au-Au, and Cu-Au interactions are plotted across the range $x<x_1$ and $x>x_2$ in Fig. 1. It can be seen that Au acts as an oversized substitutional solute in copper.

The choice of the universal potential, the construction of the exponential potential, and the adjustment of coefficient a_6^{AA} for pure Cu, and the addition of the fourth node r_4^{AB} for the Cu-Au cross potential, are totally determined by the requirement of the problem considered, i.e., the potential being used must be valid for high-energy collisions in the range less than the nearest neighbor distance where the original potentials derived by Ackland et al.[21] and developed further by Ackland and Vitek[13] are unsound. It should be emphasized that the modifications made here do not affect the fit to the pure metal and alloy properties used by Ackland and Vi-

tek[13] in deriving the original potentials for the Cu-Cu, Cu-Au, and Au-Au systems. Foreman, English, and Phythian[7] have also developed a potential for damage simulations of pure Cu by modifying the original Cu-Cu pair function of Ackland et al.,[21] but in a slightly different way from that described here. The resulting pair interaction is slightly less hard than the potential used here, as shown in Fig. 1, but both give a similar pressure response for the perfect crystal, as can be seen from Fig. 2, where pressure P is expressed in units of kT_m/Ω_0 and volume per atom Ω is in units of Ω_0; here Ω_0 is the volume per atom ($=a_0^3/4$) for a perfect crystal under zero pressure, k is Boltzmann's constant, and T_m the equilibrium melting point. (For Cu, $kTm=0.117$ eV and $kT_m/\Omega_0=1.587$ GPa.) We also include data for the unmodified Cu-Cu potential for Ackland and Vitek,[13] the empirical relationship of Rose et al.,[22] which is often used for fitting parameters in embedded-atom potentials, and experiments on copper. Generally, the modifications made here are good.

It is easy to show that the contribution of the many-body potential in Eq. (1) to interatomic energy and force becomes far and away smaller than that from the pair term as interatomic spacing is reduced below the equilibrium nearest-neighbor spacing of $a_0/\sqrt{2}$. Therefore, no modification is needed for the many-body parts and their original forms are kept. The numerical values for the parameters in these functions are to be found in Ref. 13.

III. POINT DEFECTS

A. Definitions of defect formation energies and volumes

There exists considerable ambiguity about the definition of the energy of defect in alloys, as discussed in
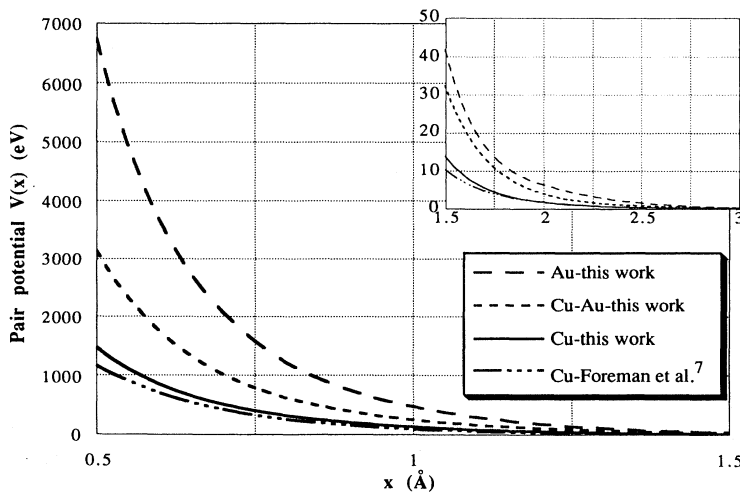
FIG. 1. Variation of the pairwise function $V(x)$ for Cu-Cu, Cu-Au, and Au-Au interactions, as indicated. The Cu-Cu potential developed by Foreman et al. (Ref. 7) is also shown for comparison.
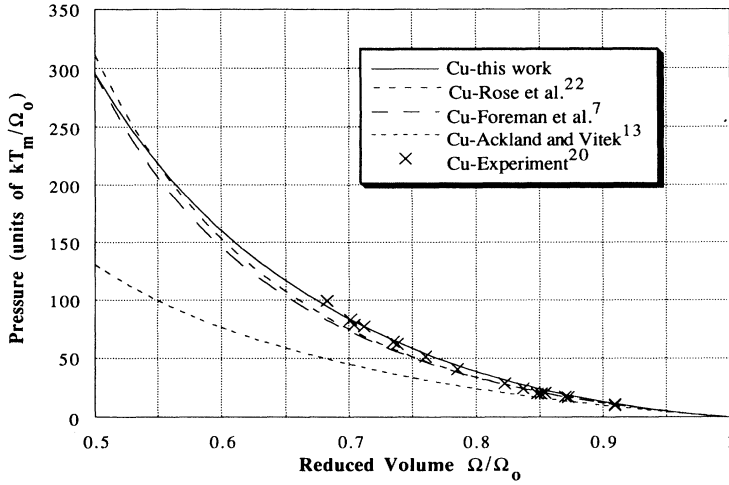
FIG. 2. The pressure-volume relationship for a perfect copper crystal described by the Cu-Cu potentials developed here and in Refs. 7 and 13. (Interactions out to second neighbors only are included, to be consistent with the potential range for a perfect crystal in equilibrium at zero pressure. These are the dominant interactions at all volumes.) The empirical form derived by Rose et al. (Ref. 22) and experimental data for copper (Ref. 20) are shown for comparison.

some detail by Ackland.[23] This is mainly due to the question as to what is the proper reference state to calculate the energy. Therefore it is necessary to give a clear definition of the defect energy calculated in simulation studies such as this. For pure material and dilute alloys, formation energies for the vacancy and interstitial can be calculated with a unified formula as follows:

$$E^f_{\text{defect}} = E^N_{\text{block}} - N_A \varepsilon_A - N_B \varepsilon_B \ , \tag{7}$$

where E^N_{block} is the total energy (negative) acquired by simulating a block of atoms containing the defect, N_A A-type hosts and $N_B (\ll N_A)$ B-type guests, with a total of $N (= N_A + N_B)$ atoms; ε_A is the energy (negative) per atom in the pure metal, and ε_B is defined as

$$N_B \varepsilon_B = E^{N^0}_{\text{block}} - N^0_A \varepsilon_A \ , \tag{8}$$

where $E^{N^0}_{\text{block}}$ represents the total energy (negative) acquired by simulating a block of N^0 atoms containing no defect, N^0_A A type solvent atoms and N_B B type substitutional solute atoms. In the dilute case, $N_B \ll N^0_A (\cong N_A)$, and thus, in the present work, where $N^0_A = 3999$ and $N_B = 1$ is much much less than N^0_A, definition (8) is valid. Likewise the formation volumes for the vacancy and interstitial can be defined as

$$V^f_{\text{defect}} = V^N_{\text{block}} - N_A \Omega_A - N_B \Omega_B \ , \tag{9}$$

with

$$N_B \Omega_B = V^{N^0}_{\text{block}} - N^0_A \Omega_A \ , \tag{10}$$

where these volume terms are defined in the same way as their energy counterparts above.

Equations (7)–(10) clearly define the defect formation energies and formation volumes. In particular, when $N_B = 0$, i.e., the crystal consists of only a single constituent, they reduce exactly to those for pure material, and, therefore, they represent a unified set. In fact, the expressions (7) and (9) for defect formation energy and volume are generally valid, not only for pure or disordered dilute systems, but also for concentrated or ordered alloy systems[23] as long as the quantities ε_A, Ω_A, ε_B, Ω_B are properly defined. Merging Eqs. (7) and (8) we have a single expression for the defect formation energy:

$$E^f_{\text{defect}} = (E^N_{\text{block}} - E^{N^0}_{\text{block}}) - (N_A - N^0_A)\varepsilon_A \ , \tag{11}$$

and likewise for the defect volume,

$$V^f_{\text{defect}} = (V^N_{\text{block}} - V^{N^0}_{\text{block}}) - (N_A - N^0_A)\Omega_A \ . \tag{12}$$

Formally, the two expressions do not depend explicitly on the quantities related to the solute B and only depend on quantities related to the solvent A, and these computable block quantities and their physical implication can easily be understood by noting that $|N - N^0| \equiv |N_A - N^0_A| \equiv$ defect number.

TABLE II. Properties of single and divacancies for pure Cu. The experimental data are from the tabulated review of Ackland et al. (Ref. 21).

	E^f_v (eV)	V^f_v (Ω_0)	E^f_v (expt.) (eV)	V^f_v (expt.) (Ω_0)
Present work	1.208	0.80	1.17–1.29	0.75–0.85
Ref. 21	1.191	0.77	1.17–1.29	0.75–0.85

	E^f_{2v} (eV)		Binding energy (eV)		V^f_{2v} (Ω_0)	
	$1/2\langle 110\rangle$	$\langle 100\rangle$	$1/2\langle 110\rangle$	$\langle 100\rangle$	$1/2\langle 110\rangle$	$\langle 100\rangle$
Present work	2.2514	2.4389	0.1639	−0.0236	1.6339	1.5984
Ref. 21	· · ·	· · ·	0.1659	−0.0335	· · ·	· · ·

TABLE III. Properties of the SIA in pure Cu.

SIA configuration	Formation energy (eV)		Formation volume (Ω_0)	
	Present work	Ref. 21	Present work	Ref. 21
$\langle 100 \rangle$ dumbbell	4.009	3.62	1.944	
$\langle 110 \rangle$ dumbbell	4.253	Unstable	1.792	
$\langle 110 \rangle$ crowdian	4.265	3.84	1.810	
Octahedral	Unstable	3.68		
Two-nearest neighbor $\langle 100 \rangle$ dumbbells	6.893		3.375	
	(Binding energy: 1.1253)			

B. Pure Cu

In the pure Cu system, the single-vacancy formation energy, E_v^f, and formation volume, V_v^f, are slightly different from the original values of Ackland et al.[21] (see Table II) but E_v^f still lies in the range of experiment.[21,24–27] Two nearest-neighbor vacancies attract each other with a binding energy of 0.164 eV, whereas two second-neighbor vacancies repel with a binding energy of -0.024 eV (see Table II).

For the single self-interstitial atom (SIA) there are only three stable configurations. Among them, the most stable is the $\langle 100 \rangle$ dumbbell, which is consistent with experimental observation by Ehrhart[24] and other studies by Koehler,[25] Young,[26] and Okuda and Mizubayashi.[27] Unlike the finding of Ackland et al.,[21] the $\langle 110 \rangle$ dumbbell is the second most stable configuration here, while the octahedral is not stable and relaxes to the $\langle 100 \rangle$ configuration. The least stable configuration is the $\langle 110 \rangle$ crowdian. The $\langle 111 \rangle$ dumbbell and tetrahedral defects are both unstable and evolve to the $\langle 100 \rangle$ configuration. Two nearest-neighbor $\langle 100 \rangle$ dumbbells attract each other with a binding energy of 1.125 eV. The values of formation energy and volume for the stable SIA configurations are shown in Table III.

C. Dilute Cu-Au alloy

As a starting point for understanding the basic properties of defects, the displacement threshold energy, and cascade structure in alloy systems, it is necessary to consider the limiting case of one single Au solute in an otherwise pure Cu lattice. In this case, there are various defect configurations to consider. First of all, E_v^f and V_v^f acquired by creating a vacancy at the solute site are exactly the same as those in the pure system, and the same holds true for the nearest-neighbor Au-Cu divacancy and for the second-neighbor Au-Cu divacancy. When the Au atom is introduced into the various interstitial positions in the Cu matrix, only two configurations are found to be stable, namely the $\langle 110 \rangle$ crowdian and the octahedral. Their respective formation energy and volume are 4.788 and 4.987 eV and 2.21 and 2.45 Ω_0. All the other Au interstitial configurations eventually turn on relaxation into a Au substitutional atom and a Cu interstitial.

Figures 3(a)–3(d) show schematic diagrams of the configurations we have considered for interaction between a Au solute and mono and divacancies; they are (a)

the nearest-neighbor vacancy, (b) the second-nearest-neighbor vacancy, (c) the nearest-neighbor stable divacancy, and (d) the near-neighbor metastable divacancy. The binding energy and formation volume of these Au solute-vacancy clusters are presented in Table IV. From the sign of the binding energies it can be seen that the solute exerts an attraction to its nearest-neighbor Cu vacancy [Fig. 3(a)] and repels its second-neighbor Cu vacancy [Fig. 3(b)]. For the cases of Figs. 3(c) and 3(d), the Au solute attracts the divacancy (positive binding energy) in both cases and the formation energies of both are lower than in pure Cu. Nevertheless, only the nearest-neighbor divacancy [Fig. 3(c)] has its divacancy binding energy increased over its value of 0.164 eV in pure copper by the presence of the Au solute.

Figure 4 shows schematically various possible Au solute–Cu interstitial configurations in near-neighbor positions. For a $\langle 100 \rangle$ Cu-Cu dumbbell centered on a nearest-neighbor site to a Au solute [Figs. 4(a) and 4(b)], the configuration in which the two copper atoms are symmetrically disposed with respect to the solute [Fig. 4(b)] is the most stable with a binding energy of 0.266 eV; the other two dumbbell orientations [Fig. 4(a)] are metastable, with a negative binding energy of -0.057 eV, and rotate by about 7.36° off the precise $\langle 100 \rangle$ axis, as illustrated in the figure. For the $\langle 100 \rangle$ dumbbells centered on second-neighbor sites to the solute [Figs. 4(c) and 4(d)], all three dumbbell orientations result in attractive configurations with binding energies of 0.058 eV for the

(a)   (b)

● Cu

● Au

⌗ Vacancy

(c)   (d)
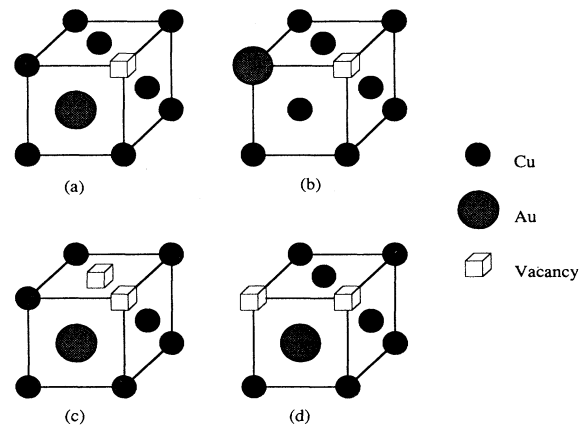
FIG. 3. Schematic illustration of the solute-vacancy arrangements considered in Table V.

TABLE IV. Properties of the vacancy-solute configurations shown in Fig. 3.

Configuration [shown in Fig. (3)]	$E_{v\text{-}Au}^b$ (eV)	E_{2v}^b (eV)	Formation energy (eV)	Formation volume (Ω_0)
3(a)	0.065		1.143	0.727
3(b)	−0.026		1.234	0.800
3(c)	0.144	0.178	2.107	1.438
3(d)	0.124	−0.029	2.315	1.455

two "transverse" states [Fig. 4(c)] and 0.074 eV for the "longitudinal" one [Fig. 4(d)]. For a $\langle 110 \rangle$ Cu-Cu dumbbell centered on a nearest-neighbor site to a Au solute, the configuration of Fig. 4(e), in which the two copper atoms are symmetrically disposed with respect to the solute, displays attraction with a binding energy of 0.123 eV, whereas the other [Fig. 4(f)] is repelled and the dumbbell moves away from its initial position by $\sqrt{2}a_0$, as illustrated, before reaching a metastable state with a binding energy of −0.052 eV. The formation energy and volume for each Cu interstitial configuration in this system are listed in Table V.

D. Discussion

The modifications to the pair part of the many-body potentials for short-range interactions have a slight influence on vacancy properties as seen in Table II, but the value for E_v^f is still well within the experimental range, as noted above in Sec. II B. The effect on the SIA is larger, as expected, since this defect involves smaller interatomic separations and our modifications have "har-

dened" the pairwise repulsion term in the potential energy. Despite the 10% difference in E_i^f (Table III), both sets of potentials predict the $\langle 100 \rangle$ dumbbell to be the most stable SIA, which is consistent with the generally accepted structure as observed above. Mixed Cu-Au interstitial dumbbells are not found to occur, however, for the crowdion and octahedral sites are the only stable configurations for the large Au interstitial.

We have shown that the effect of the substitutional Au atom on intrinsic point defects in the Cu lattice is complex. This is due to the fact that this solute is oversized in copper, as can be deduced by the form of the three curves for the pairwise repulsion V in Fig. 1, and it produces an outward displacement of 0.0509 Å on its 12 nearest-neighbor atoms and an inward one of 0.0072 Å on its 6 second neighbors in the copper lattice. The relaxation volume associated with the introduction of the solute is 0.54 Ω_0. As a result, the vacancy-solute binding energy is positive (0.065 eV) for the nearest-neighbor arrangement and negative (−0.026 eV) for the second-neighbor one. The Cu SIA-Au solute interaction is influenced by the same effect, and the results described above can all be explained qualitatively on this basis. Thus, the binding energy is large and positive (0.266 eV) for the "transverse" orientation of the stable $\langle 100 \rangle$ Cu-Cu dumbbells at the nearest site to a Au solute and moderately large (0.123 eV) for the transverse metastable $\langle 110 \rangle$ dumbbell at the same site. The relative magnitude of the binding energy between a solute atom and either vacancies or self-interstitials may be important in defect production and evolution from cascades.

IV. DISPLACEMENT THRESHOLD ENERGY

A. Cu recoil in pure copper

The displacement threshold energy E_d has been computed as described in Sec. II A for orientations around

FIG. 4. Schematic illustration of the solute-SIA arrangements considered in Table VI.

TABLE V. Properties of various Cu interstitial Au solute configurations.

Configuration (shown in Fig. 4)	$E_{i\text{-}Au}^b$ (eV)	E_i^f (eV)	V_i^f (Ω_0)
4(a)	−0.057	4.066	1.878
4(b)	0.266	3.743	1.932
4(c)	0.058	3.951	1.902
4(d)	0.074	3.935	1.925
4(e)	0.123	4.131	1.751
4(f)	−0.052	4.305	1.748
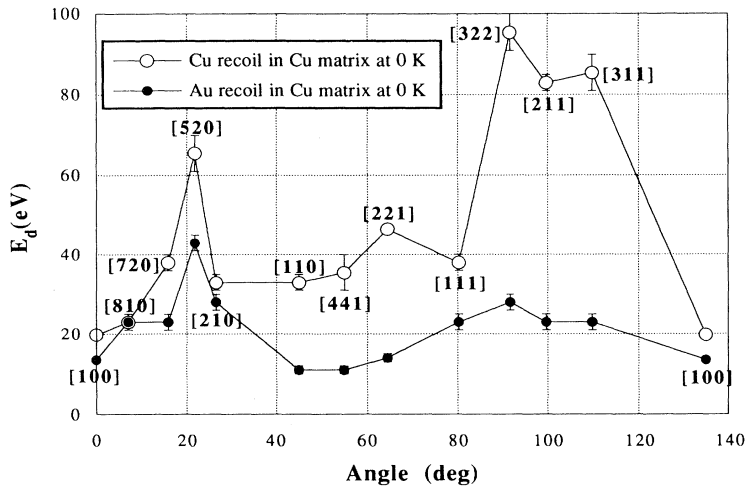
FIG. 5. The displacement threshold energy E_d (in eV) for recoil orientations around the sides of the unit stereographic triangle for both Cu and Au recoil atoms in a copper matrix at 0 K.

the outside of the unit stereographic triangle and the results for a Cu primary recoil in copper at 0 K are shown by open circles in Fig. 5. The vertical bars indicate the uncertainty in E_d as discussed in Sec. II A. It can be seen that for low-index directions in pure copper, E_d is predicted to be lowest along [100] at 20 eV, followed by orientations near [110] and then [111] at 33 and 38 eV, respectively. There is a peak of 65 eV at [520] between [100] and [110], and a broad range of orientations with high E_d also occurs between [100] and [111], with the maximum of 96 eV arising at [322].

The E_d values for pure copper along directions between [100] and [210] are similar to those deduced from low-temperature electron irradiations by King, Merkle, and Meshi,[28] but are higher (by about 10 eV) at [110], and are significantly lower and higher near [111] and [211], respectively. Hohenstein, Seeger, and Sigle[29] have argued that E_d for copper is actually lowest (at about 18 eV) near ⟨110⟩, but our model does not show that. Foreman, English, and Phythian[7] have recently computed E_d in the orientations between [100] and [110] for copper using their modification of the many-body potential of Ackland et al.[21] mentioned in Sec. II B. From a value of 18 eV at [100] their E_d values rise to 66 eV near [520] and fall to 28 eV at [110]. Spot values in the region of [111] were found to be 60–80 eV. There is therefore reasonable agreement between the two sets, and, since the two MD codes were essentially the same, the differences in E_d must reflect a sensitivity to the precise details of the interatomic potential inside the nearest-neighbor spacing. In a parallel MD study of E_d in pure copper at 0 K, Chou and Ghoniem[19] used a potential based on the embedded-atom model,[10] but modified it at small interatomic separations in a very similar manner to the procedure used here and in Ref. 18. Their values for E_d between ⟨100⟩ and ⟨110⟩ and between ⟨100⟩ and ⟨111⟩ are similar to those given here in Fig. 5. However, their value at ⟨111⟩ of about 70 eV, and even higher values between ⟨111⟩ and ⟨110⟩, are somewhat larger than our own. Despite the differences in detail between the results of these recent simulations, they can be considered to offer broad agreement, particularly in view of the

differences of the potentials employed. All three sets differ in one respect to the earlier simulation study by King and Benedek[30] using the Gibson-II nonequilibrium pair potential for copper. In their work, E_d at ⟨111⟩ was 100 eV and even higher peaks with values of 150–170 eV were found on either side of that orientation. However, threshold energies of this magnitude have not been obtained with the more realistic potentials, and we conclude that the data for pure copper obtained here are sufficiently close to those from experiment, which in any case is not for 0 K, and other modeling, that they are meaningful.

The minimum along [100] is achieved by a short sequence of only 3 atomic replacements, whereas E_d for [110] is sufficient to produce a RCS of 15 replacements. The threshold for [111] is achieved when the primary recoil atom can overcome the repulsion of its three neighbors and form a metastable octahedral SIA at the position 1/2[111]. The high E_d values between [100] and [110] and between [100] and [111] arise from the fact that primary recoils in these directions generate multiple, but short, ⟨110⟩ RCS, and a stable Frenkel pair is not created until sufficient energy is imparted to one of these sequences. Generally, we observe that the size of E_d is related to the maximum number of atoms displaced, even if only temporarily, from their sites by the recoil event, as found for other crystal structures.[31]

B. Au recoil in otherwise pure copper

The variation of E_d with recoil orientation for a Au recoil in otherwise pure copper at 0 K is shown by filled circles in Fig. 5. The most notable feature of the results is that E_d for a Au recoil atom in copper is generally much lower than that of a Cu self-atom and has a much smaller variation with recoil direction. For this heavy, oversized solute, E_d is marginally lower for [110] than [100] (11 eV cf. 13 eV), although a peak still exists between these two minima. The biggest effect of changing the recoil species, however, is seen to occur between [100] and [111], for the E_d values in this part of stereographic triangle are not the highest for the Au recoil and the

high, broad peak around [211] does not exist in the dilute Cu-Au alloy. As noted in the preceding section, atomic interactions in the energy range of E_d are influenced by modifications to the pair term in the potential, and since the potential parameters can only be fitted to physical properties with firm confidence at near-equilibrium atomic separations, the computed E_d values have an element of uncertainty in their magnitude. However, since we are mainly concerned here with the effect on E_d when the recoil atom changes from Cu to Au, we believe the effects found, and particularly that the E_d values for a Au primary recoil atom are uniformly low, are meaningful. These results illustrate the possible importance of mass and size effects in alloys. For all the directions considered here, the Au recoil left its site at the threshold and occupied another substitutional site by displacing a Cu atom. As a consequence, the process of recombination of a newly formed Cu interstitial with the vacancy was hindered by the immobile, oversized Au solute. Thus, despite the low efficiency of kinetic-energy transfer engendered by the large mass difference of the two atomic species, this blocking mechanism provides a means of achieving stable Frenkel pairs at low energy. As a consequence, the number of atomic replacements was only 2 and 5 for the [100] and [110] directions, respectively.

C. Discussion

It is well known, and was commented upon in Sec. II A, that focused collision sequences are a feature of low-energy collisions in directions of closely packed atomic rows in metals, and at the displacement threshold, the RCS process can result in stable Frenkel pair production by depositing the SIA well away from the vacant site. RCS have a part to play in separating SIA from vacancies in displacement cascades, but it is not clear what effects solutes have on this process in general. We have seen above that in changing from a Cu to a Au primary recoil in copper, the threshold RCS is reduced from 15 to 5 replacements for $\langle 110 \rangle$, with an approximately proportional reduction in E_d. This effect arises from the first replacement step in the sequence when the Au primary re-

places a Cu atom, a change that is difficult to undo as the atoms in the chain recoil in the reverse direction. It is of interest, therefore, to investigate the influence of a single Au solute on RCS events in its vicinity, even when the primary recoil is a Cu atom.

We have done this by simulating $\langle 110 \rangle$ and $\langle 100 \rangle$ collision chains in copper with a Au solute substituted for a Cu atom either along the chain or in an adjacent atomic row on the same $\{001\}$ plane. As before, E_d was determined from the recoil energy that produced a stable Frenkel pair. The results are shown in Fig. 6, where E_d is plotted as a function of the distance (in replacement lengths) of the Au solute from the primary Cu site projected onto the $\langle 100 \rangle$ or $\langle 110 \rangle$ axis in question. Row 0 indicates that the solute is in the same atomic row as the collision sequence, and Row 1 or Row 2 indicate that it is in the nearest or second-nearest atomic row to the sequence. The data points show that recoil energies at which stable Frenkel pairs were produced, and the points at the bottom of the uncertainty bars are the highest energy at which stable pairs were not produced.

For the $\langle 110 \rangle$ events, for which 15 replacements were produced by the threshold RCS at 35 eV in pure copper, it can be seen that E_d is unchanged when the Au atom is at site 12 for Row 0, but as the separation between the primary Cu atom and the Au site is reduced, E_d is affected in a substantial manner by the same replacement and blocking mechanism described above. The effect is less pronounced for Row 1, although there is still a sizable reduction in E_d. In this case, it is brought about not by a displacement of the solute but by the obstructive effect it has on the return of the replacement chain in the adjacent $\langle 110 \rangle$ row.

For the $\langle 100 \rangle$ recoil, the influence of the Au solute is much shorter in range and more complex, presumably because energy propagation is less focused for this direction. It can be seen that when the Au solute lies on the $\langle 100 \rangle$ RCS row at sites 1 and 2, E_d is increased well above the pure copper value of 20 eV because of the difficulty the primary Cu recoil has in displacing the oversized atom from its site. At and beyond the RCS range in pure copper (three replacements), the solute has
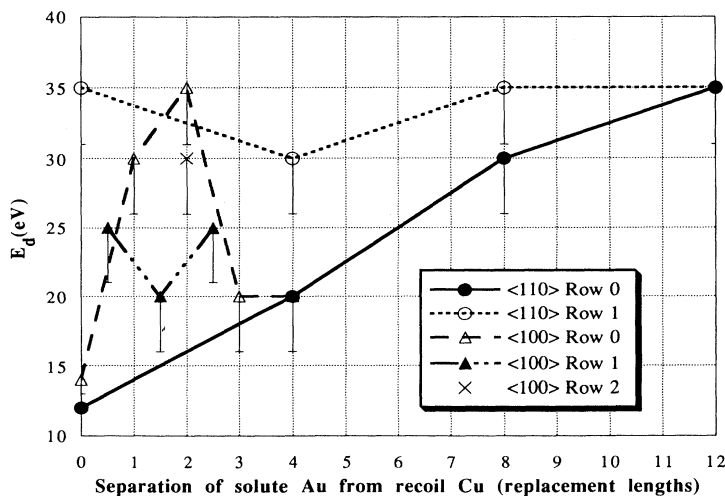
FIG. 6. Illustration of the influence of a substitutional Au solute atom on the RCS threshold event for $\langle 110 \rangle$ and $\langle 100 \rangle$ directions. (The unit replacement length is $a_0/\sqrt{2}$ and a_0 for $\langle 110 \rangle$ and $\langle 100 \rangle$, respectively.)

no effect. When the Au atom lies in the adjacent $\langle 100 \rangle$ row, the effect on E_d is smaller, but the increase in E_d seen for two of the Au sites arises because this oversized atom disrupts the $\langle 100 \rangle$ collision chain and makes it more difficult to propagate. We have only considered one site for the Au atom in the second-neighbor $\langle 100 \rangle$ row, and here, there is a significant increase in E_d. This is because the large outward displacements of the nearest-neighbor atoms to the solute tend to close the $\langle 100 \rangle$ channel of the collision chain, and hence, increase the energy required to produce a stable Frenkel pair in this direction.

It can be seen, therefore, that the influence of solute atoms on the threshold displacement process is complex. As a primary recoil atom, the heavy, oversized species considered here results in a reduction in the energy for defect production, but the presence of these solutes in the vicinity of solvent recoil atoms affects the threshold in different ways. For the RCS mechanism along the close-packed $\langle 110 \rangle$ direction, the solutes reduce both the energy and length of the threshold event. We have not yet treated other species of substitutional solute, but would expect mass to be less important than size for the defect

properties considered here. For this reason, the replacement and blocking process described above may not be quite so important for undersized solutes, since the energy required to move them from site to site in a collision chain may be less. These points require further study. The main aim of our research is to investigate the role of solute atoms in defect production in displacement cascades. We are using the Cu-Au system as a model alloy for this, and have presented preliminary results on cascades of up to 0.5 keV in Ref. 32. We have more recently extended this work to cascade energies of up to 2 keV, and the results of these simulations will be presented in due course.

ACKNOWLEDGMENTS

[1]T. Diaz de la Rubia and W. J. Phythian, J. Nucl. Mater. **191-194**, 108 (1992).

[2]A. Caro, M. Victoria, and R. S. Averback, J. Mater. Res. **5**, 1409 (1990).

[3]F. Gao and D. J. Bacon, Philos. Mag. A **67**, 275 (1993).

[4]F. Gao and D. J. Bacon, Philos. Mag. A **67**, 289 (1993).

[5]T. Diaz de la Rubia, A. Caro, and M. Spaczer, Phys. Rev. B **47**, 11 483 (1993).

[6]T. Diaz de la Rubia and M. W. Guinan, J. Nucl. Mater. **174**, 151 (1990).

[7]A. J. E. Foreman, C. A. English, and W. J. Phythian, Philos. Mag. A **66**, 655 (1992).

[8]A. J. E. Foreman, W. J. Phythian, and C. A. English, Philos. Mag. A **66**, 671 (1992).

[9]M. W. Finnis (unpublished).

[10]M. S. Daw and M. J. Baskes, Phys. Rev. B **29**, 6443 (1984).

[11]M. W. Finnis and J. W. Sinclair, Philos. Mag. A **50**, 45 (1984).

[12]J. G. Ackland, M. W. Finnis, and V. Vitek, J. Phys. F **18**, L153 (1988).

[13]G. J. Ackland and V. Vitek, Phys. Rev. B **41**, 10 324 (1990).

[14]J. P. Biersack and J. F. Ziegler, J. Nucl. Instrum. Methods **141**, 93 (1982).

[15]W. Eckstein, in *Computer Simulation of Ion-Solid Interactions*, Springer Series in Materials Science Vol. 10 (Springer-Verlag, Berlin, 1991), Chap. 4.

[16]W. Hetterich, H. Derks, and W. Heiland, Nucl. Instrum. Methods **33**, 401 (1988).

[17]W. Eckstein and M. Hou, Nucl. Instrum. Methods **31**, 386 (1988).

[18]S. Pronnecke, A. Caro, M. Victoria, T. Diaz de la Rubia, and M. W. Guinan, J. Mater. Res. **6**, 483 (1991).

[19]S. P. Chou and N. M. Ghoniem, J. Nucl. Mater. **171-181**, 909 (1991).

[20]R. Kinslow, *High-Velocity Impact Phenomena* (Academic, New York, 1970).

[21]G. J. Ackland, G. Tichy, V. Vitek, and M. W. Finnis, Philos. Mag. A **56**, 735 (1987).

[22]J. H. Rose, J. R. Smith, F. Guinea, and J. Ferrante, Phys. Rev. B **29**, 2963 (1984).

[23]G. J. Ackland, Philos. Mag. A **67**, 285 (1993).

[24]P. Ehrhart, J. Nucl. Mater. **69-79**, 200 (1978).

[25]J. S. Koehler, in *Point Defects and Defect Interactions in Metals* (Tokyo University Press, Tokyo, 1982), p. 143.

[26]F. W. Young, J. Nucl. Mater. **69-70**, 310 (1978).

[27]S. Okuda and H. Mizubayashi, in *Point Defects and Defect Interactions in Metals* (Ref. 25), p. 163.

[28]W. E. King, K. L. Merkle, and M. Meshi, J. Nucl. Mater. **117**, 12 (1983).

[29]M. Hohenstein, A. Seeger, and W. Sigle, J. Nucl. Mater. **169**, 33 (1989).

[30]W. E. King and R. Benedek, J. Nucl. Mater. **117**, 26 (1983).

[31]D. J. Bacon, A. Calder, and S. Wooding, J. Nucl. Mater. (to be published).

[32]Hui-fang Deng and D. J. Bacon, Radiat. Eff. Def. Solid (to be published).